Received: 15 May 2019 | Revised: 16 July 2019 | Accepted: 29 July 2019

DOI: 10.1002/jbio.201900197

FULL ARTICLE

JOURNAL OF BIOPHOTONICS

Fast and sensitive delineation of brain tumor with clinically compatible moxifloxacin labeling and confocal microscopy

Seunghun Lee[1] | Won Yeong Park[1] | Hoonchul Chang[2] | Bumju Kim[2] | Won Hyuk Jang[2] | Seonghan Kim[1] | Younghoon Shin[6] | Myoung Joon Kim[3] | Kyung Hwa Lee[4] | Eui Hyun Kim[5] | Euiheon Chung[6] | Ki Hean Kim[1,2]*

[1]Department of Mechanical Engineering, Pohang University of Science and Technology, Pohang, Gyeongbuk, Republic of Korea

[2]Division of Integrative Biosciences and Biotechnology, Pohang University of Science and Technology, Pohang, Gyeongbuk, Republic of Korea

[3]Department of Ophthalmology, University of Ulsan College of Medicine, Asan Medical Center, Seoul, Republic of Korea

[4]Department of Pathology, Chonnam National University Medical School, Chonnam National University Hwasun Hospital, Hwasun-gun, Jeonnam, Republic of Korea

[5]Department of Neurosurgery, Yonsei University College of Medicine, Severance Hospital, Seoul, Republic of Korea

[6]Department of Biomedical Science and Engineering, Gwangju Institute of Science and Technology, Gwangju, Republic of Korea

***Correspondence**
Ki Hean Kim, Department of Mechanical Engineering and Division of Integrative Biosciences and Biotechnology, Pohang University of Science and Technology, 77 Cheongam-ro, Nam-gu, Pohang, Gyeongbuk 37673, Republic of Korea.
Email: kiheankim@postech.ac.kr

Funding information
Industrial Technology Innovation Program, Grant/Award Number: 10048358; Research grant, National Research Foundation of Korea, Grant/Award Number: NRF-2016R1A2B4015381; the Brain Research Program, National Research Foundation of Korea, Grant/Award Number: NRF-2017M3C7A 1044964; the Korea-Sweden Research Cooperation Program, Grant/Award Number: 2017R1A2A1A18070960

Abstract

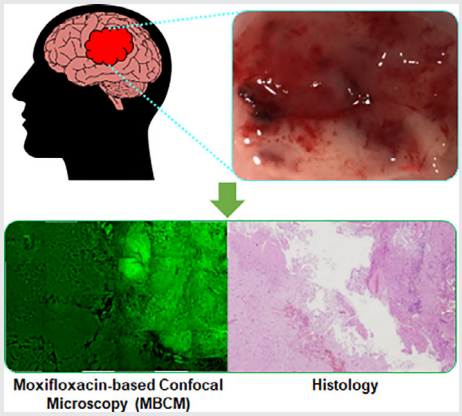

Delineation of brain tumor margins during surgery is critical to maximize tumor removal while preserving normal brain tissue to obtain optimal clinical outcomes. Although various imaging methods have been developed, they have limitations to be used in clinical practice. We developed a high-speed cellular imaging method by using clinically compatible moxifloxacin and confocal microscopy for sensitive brain tumor detection and delineation. Moxifloxacin is a Food and Drug Administration (FDA) approved antibiotic and was used as a cell labeling agent through topical administration. Its strong fluorescence at short visible excitation wavelengths allowed video-rate cellular imaging. Moxifloxacin-based confocal microscopy (MBCM) was characterized in normal mouse brain specimens and visualized their cytoarchitecture clearly. Then, MBCM was applied to both brain tumor murine models and two malignant human brain tumors of glioblastoma and metastatic cancer. MBCM detected tumors in all the specimens by visualizing dense and irregular cell distributions, and tumor margins were easily delineated based on the cytoarchitecture. An image analysis method was developed for automated detection and delineation. MBCM demonstrated sensitive delineation of brain tumors through cytoarchitecture visualization and would have potentials for human applications, such as a surgery-guiding method for tumor removal.

KEYWORDS
anti-bacterial agents, brain neoplasms, confocal microscopy, fluorescence, topical administration

1 | INTRODUCTION

Malignant brain tumor is a fatal cancer that leads to finite patient survival owing to recurrence. Surgical resection is the primary treatment method for most malignant brain tumors. The more tumor resection is related to longer patient survival [1]. However, extensive resection also increases the possibility of neurological deficits [2], and this decreases the quality of life and leads to poor treatment outcome. Therefore, complete resection of tumor tissue while preserving normal brain tissue is critical to obtain an optimal clinical outcome. Currently, brain tumor margins are determined based on visual inspection of surgeons and anatomical information from medical imaging methods such as computerized tomography [3], magnetic resonance imaging [4], and intraoperative ultrasound [5]. Although medical imaging methods provide crucial information for tumor localization, they are not reliable in terms of precise tumor margin delineation. Real-time and high-sensitivity detection methods are useful for demarcating brain tumors, and various optical imaging methods are developed. Wide-field fluorescence imaging methods using intravenously injectable indocyanine green (ICG) [6] and orally administered 5-aminolevulinic (5-ALA) [7] are currently used in the surgery for real-time tumor detection. Although these fluorophores help to detect the presence of tumors, interpretation of the imaging result largely depends on surgeon's impression of fluorescence intensity. Additionally, the methods do not exhibit enough sensitivity for brain tumor delineation. High-resolution imaging methods at the cellular level could aid in improving the sensitivity of the fluorescence imaging methods. Confocal laser endomicroscopy (CLE) visualizes cells with micron-level resolution and has been tested in clinics [8]. However, the image contrast was limited partly due to difficulty in fluorophore delivery which requires disruption of the brain-blood barrier [9, 10].

Various label-free optical imaging techniques have been developed to enable the sensitive delineation of tumor margin. Optical coherence tomography (OCT) is an imaging technique based on light back-scattering and it detected tumors based on decreased light scattering and microstructure change [11]. However, OCT provides limited contrasts and resolution for the sensitive delineation of tumor margins. Coherent Raman scattering (CRS) microscopy is based on intrinsic Raman scattering of molecules including lipids and proteins and it detected brain tumors based on either decreased lipid Raman scattering or increased protein Raman scattering [12, 13]. These changes in Raman scattering in tumors were associated with the disruption of normal brain cellular structure including myelinated axons and the expansion of cancer cells. Although CRS microscopy methods provided good chemical specificity and imaging speeds for tumor margin delineation, the methods are costly owing to the need for pico-second pulse lasers as light sources, and the implementation of small imaging devices is technically challenging. We recently reported on moxifloxacin-based two-photon and coherent anti-Stokes Raman scattering (CARS) combined microscopy that could detect brain tumors and demarcate tumor margins based on cellular structure and lipid Raman scattering [14]. Moxifloxacin is an antibiotic that is used for the treatment and prevention of ocular and pulmonary infection in clinic [15, 16] and is known to exhibit intrinsic fluorescence through ultra-violet (UV) excitation [17]. We found that moxifloxacin could fluoresce through nonlinear two-photon [18] and three-photon excitation [19] using near-infrared wavelengths and label cells inside the tissue with good tissue and cell penetration. With moxifloxacin labeling, two-photon microscopy (TPM) imaged cells in various tissues approximately 10 times faster when compared to cases without labeling, and brain tumors were detected based on their different cellular structures such as high cell density and irregular cell arrangement. However, the imaging speed of moxifloxacin-based TPM was still limited owing to the low efficiency of two-photon excitation. With respect to clinical application, the enhancement in imaging speed is essential to moxifloxacin-based cellular imaging for the rapid screening of clinically meaningful large tissue sections. Additionally, femtosecond pulse lasers for TPM are expensive and sensitive to environmental changes in temperature and humidity. Thus, the development of two-photon imaging devices for clinical applications is challenging.

In this study, we explored the potential of high-speed cellular imaging based on moxifloxacin and its single-photon excitation for brain tumor detection and delineation. The imaging speed can be significantly enhanced by using single-photon excitation, which is usually considerably more efficient than two-photon excitation. Additionally, continuous-wave lasers for single-photon excitation are inexpensive and less sensitive to the environments than the femtosecond lasers for two-photon excitation. Miniaturized confocal imaging devices such as CLE are also commercially available. In this study, single-photon excitation/emission spectra and fluorescence intensity of moxifloxacin were initially characterized. Subsequently, high-speed confocal microscopy using single-photon excitation of moxifloxacin was tested and analyzed in normal mouse brain tissues. Following the characterization in the normal brain tissues, moxifloxacin-based confocal microscopy (MBCM) was applied to brain tumor mouse models and human brain tumor tissues to test the feasibility of brain tumor cell detection and tumor margin delineation. An image processing algorithm was developed based on the acquired image data for automated detection.

2 | MATERIALS AND METHODS

2.1 | Confocal microscope system

A commercial confocal microscopy system (SP-5, Leica) was used for imaging moxifloxacin labeled brain samples. The system has multiple continuous wave (CW) lasers covering the wavelength from 405 to 633 nm. Emission light was spectrally resolved up to five channels by using a prism and moving slits. Either a 20× objective lens (Water immersion, NA 1.0, HCX APO L, Leica) or a 10× objective lens (Dry, NA 0.3, HC PL FLUOTAR, Leica) was used. The imaging speed was from 0.27 to 29.4 frames/second for 512 × 512-pixel images.

2.2 | Characterization of fluorescence properties of moxifloxacin ophthalmic solution

For excitation spectrum measurement, moxifloxacin ophthalmic solution (Vigamox, Alcon) was diluted to 0.8 μM with phosphate buffered saline (PBS). The diluted moxifloxacin solution (1 mL) was transferred to a cuvette and measured with a spectrophotometer (RF5301pc, Shimadzu). A spectral range from 440 to 665 nm was measured with the change of excitation wavelength from 250 to 430 nm with a step size of 5 nm. For the measurement of emission spectrum, moxifloxacin ophthalmic solutions were diluted to 0.6 mM with PBS and measured with the spectrophotometer. Excitation wavelength was set at 405 nm and the emission spectrum was measured from 430 to 665 nm.

Fluorescence intensity of the moxifloxacin ophthalmic solution was analyzed in comparison with a commercial fluorescence dye having similar fluorescence spectra, Hoechst 33342 solution (#62249, Thermo Fisher Scientific). Both moxifloxacin ophthalmic solutions and Hoechst 33342 solutions were diluted to 1 mM with PBS and fluorescence intensity was measured by using the commercial confocal microscopy system. The diluted solutions were transferred onto hollow glass slides and sealed with coverslips and nail polish. The solution specimens were imaged with excitation wavelength of 405 nm and a single channel detection covering from 430 to 665 nm. Average fluorescence intensity was calculated from the solution images.

2.3 | Sample preparation and MBCM imaging of normal mouse brains

Overall procedures of brain tissue preparation and MBCM imaging are shown in Figure S1. All animal experiment procedures were approved by the Institutional Animal Care and Use Committee (approval number POSTECH-2015-0030-R2) and were in compliance with the relevant regulations. For normal mouse brain samples, three C57BL/6 mice with the age of approximately 5 to 6 weeks were humanely euthanized, and brains were surgically extracted. The extracted brains were sectioned in the coronal direction with a thickness of 2 mm by using a mouse brain matrix (RBMA-200C, World Precision Instruments). The moxifloxacin ophthalmic solution was topically administrated for 5 minutes with 2.5 μL per mm^2. Subsequently, MBCM imaging was conducted. The imaging speed was 29.4 frames/second for 512 × 512-pixel images and the imaging field of view (FOV) was 387.5 × 387.5 μm^2. Excitation wavelength was 405 nm and excitation power was less than 2.3 mW. Moxifloxacin fluorescence was collected at a single channel covering from 430 to 665 nm.

In order to characterize moxifloxacin labeling of cells in the brain, a commercial cell nucleus staining dye (acridine orange) was used to co-label the brain specimen. Acridine orange solution was topically administered on mouse brain slices for 5 minutes first, and then moxifloxacin was administered for the next 5 minutes. The co-labeled mouse brain specimens were imaged by the confocal microscopy system. Moxifloxacin-based confocal imaging was conducted first, and then acridine orange-based confocal fluorescence imaging was conducted the next. Two excitation wavelengths of 405 and 496 nm were used for moxifloxacin and acridine orange, respectively, and their excitation powers were 2.3 and 1 mW, respectively. Emission light was split into two channels, 425 to 481 nm for moxifloxacin and 510 to 665 nm for acridine orange. Confocal images had the FOV of 129 × 129 μm^2 and were acquired at 2.5 frames/second.

MBCM of the normal mouse brain appeared to visualize nerves as well as cells. To confirm nerve imaging, MBCM was conducted simultaneously with reflectance confocal microscopy (RCM) which is a standard method for imaging myelinated axons on the normal mouse brain. For the simultaneous MBCM and RCM imaging, two lasers of 405 and 633 nm were used. Moxifloxacin fluorescence and reflection were collected by splitting emission light into two channels of 430 to 600 nm and 618 to 648 nm, respectively. Laser powers for MBCM and RCM were 2.3 and 0.1 mW, respectively.

2.4 | Sample preparation and MBCM imaging of brain tumor mouse models

A procedure of sample preparation and imaging is depicted in Figure S1B. Three brain tumor mouse models were generated by injecting glioblastoma cancer cells expressing DsRed fluorescent protein into the C57BL/6 mouse brains. The fluorescent cancer cells were used to map the cancer cell distribution in the brain. When cancer cells grew sufficiently in approximately 1–2 weeks post-injection, the mouse was humanely euthanized. The mouse brain was extracted, sectioned in the coronal plane, and then imaged after installing the moxifloxacin ophthalmic solution (2.5 μL per mm^2) and incubating for 5 minutes. The imaging speed was 0.4

frames/second for a 1024 × 1024-pixel image with FOV of 775 × 775 μm^2. For the simultaneous imaging of moxifloxacin and DsRed fluorescence, two excitation lasers of 405 and 561 nm were used. Emission light was split to two channels: approximately 425 to 520 nm and 580 to 660 nm for moxifloxacin and DsRed, respectively. Excitation power of the 405 nm excitation laser was 1.6 mW and that of the 561 nm excitation laser was 0.2 mW.

2.5 | Sample preparation and MBCM imaging of human brain tumor specimens

Two kinds of human brain tumor specimens of glioblastoma (n = 3) and metastatic cancer (n = 3) were provided by Yonsei Severance Hospital under the Severance Hospital Institutional Review Board (IRB# 1–2018-0049), and the samples were imaged within 12 hours of post-excision. A procedure of sample preparation and imaging is depicted in Figure S1C. After topical administration of moxifloxacin and incubation for 5 minutes, moxifloxacin-based confocal imaging was conducted in relatively large sections ranging to a few millimeters on a side to capture both tumor and tumor-neighboring regions. Once confocal imaging was completed, tissue specimens were processed for histology inspection. Excitation wavelength for moxifloxacin fluorescence was 405 nm, and the excitation power was 2.3 mW. Moxifloxacin fluorescence was collected at a single channel covering approximately 430 to 665 nm. The imaging speed was 0.4 frames/seconds for 1024 × 1024-pixel image.

2.6 | Sample preparation and MBCM imaging of mouse peripheral blood

In order to examine moxifloxacin labeling of red blood cells (RBCs) and white blood cells (WBCs), mouse peripheral blood was extracted and imaged by MBCM. About 20 μL of peripheral blood was extracted from the mouse tail vein. The extracted blood was diluted with 200 μL of PBS and stained with 200 μL of moxifloxacin. Then, 10 μL of the mixture was smeared on a glass slide and coverslipped, and MBCM imaging was performed. An excitation wavelength of 405 nm was used with 0.1 mW power. The confocal imaging was conducted at 0.27 frames/second for a 512 × 512-pixel. Fluorescence was collected at a single chancel covering from 430 to 665 nm.

2.7 | Histological examination of human brain tumor tissues

For histological examination, tissue specimens were fixed in 4% (w/v) paraformaldehyde for 24 hours and then in 10% neutral-buffered formalin for 3 days. The tissues were dissected, embedded in paraffin, and stained with hematoxylin and eosin (H&E) for histopathological evaluation. In order to assess the distribution of T-lymphocytes, immunohistochemistry using anti-human CD3 antibody (clone F7.2.38, code M7254, DakoCytomation) was performed. Then, 3-μm thick tissue sections were subject to an automated immunostainer (Leica Bond-III stainer, Leica Biosystems). Microphotographs were obtained through a microscopy (Eclipse 80i, Nikon Instruments) and NIS elements software (Human Genetics).

3 | RESULTS

3.1 | Single-photon fluorescence properties of moxifloxacin

Single-photon fluorescence properties of a commercial moxifloxacin ophthalmic solution were analyzed. The moxifloxacin ophthalmic solution was used to label brain specimens through topical administration. Excitation/emission spectra of the moxifloxacin ophthalmic solution were measured by using a spectrophotometer (Figure 1A), and the excitation spectrum exhibited two peaks in the UV wavelength range: the first and second peaks at approximately 290 and 340 nm, respectively. Excitation efficiency at over 400 nm was less than 1% of the first peak. The result was consistent with that in previous studies [16]. Emission spectrum of the moxifloxacin ophthalmic solution was measured at an excitation wavelength of 405 nm, and it exhibited a peak at approximately 500 nm with a broad full-width half maximum of approximately 90 nm. Fluorescence intensity of the moxifloxacin ophthalmic solution was analyzed in comparison with that of a commercial cell nuclear dye, Hoechst. In the fluorescence intensity comparison, a short visible wavelength of 405 nm was used as the excitation wavelength as opposed to UV wavelengths with high excitation efficiency. The short visible wavelength was used owing to its availability in the commercial confocal microscopy system as the light source although it was not optimal. Furthermore, the short visible wavelength is advantageous relative to the UV wavelengths because it minimizes potential photodamage to the sample during imaging. The fluorescence intensity of moxifloxacin ophthalmic solution was approximately six times that of Hoechst at the same concentration. Although moxifloxacin would be dimmer than Hoechst in the brain tissue owing to the fluorescence enhancement of Hoechst upon DNA binding by more than 30 times [20], moxifloxacin still exhibited significant fluorescence comparable to that of the commercial dye.

3.2 | High-speed confocal microscopy of normal mouse brains through moxifloxacin labeling

Confocal microscopy imaging of the brain tissue through moxifloxacin labeling was tested on normal mouse brain

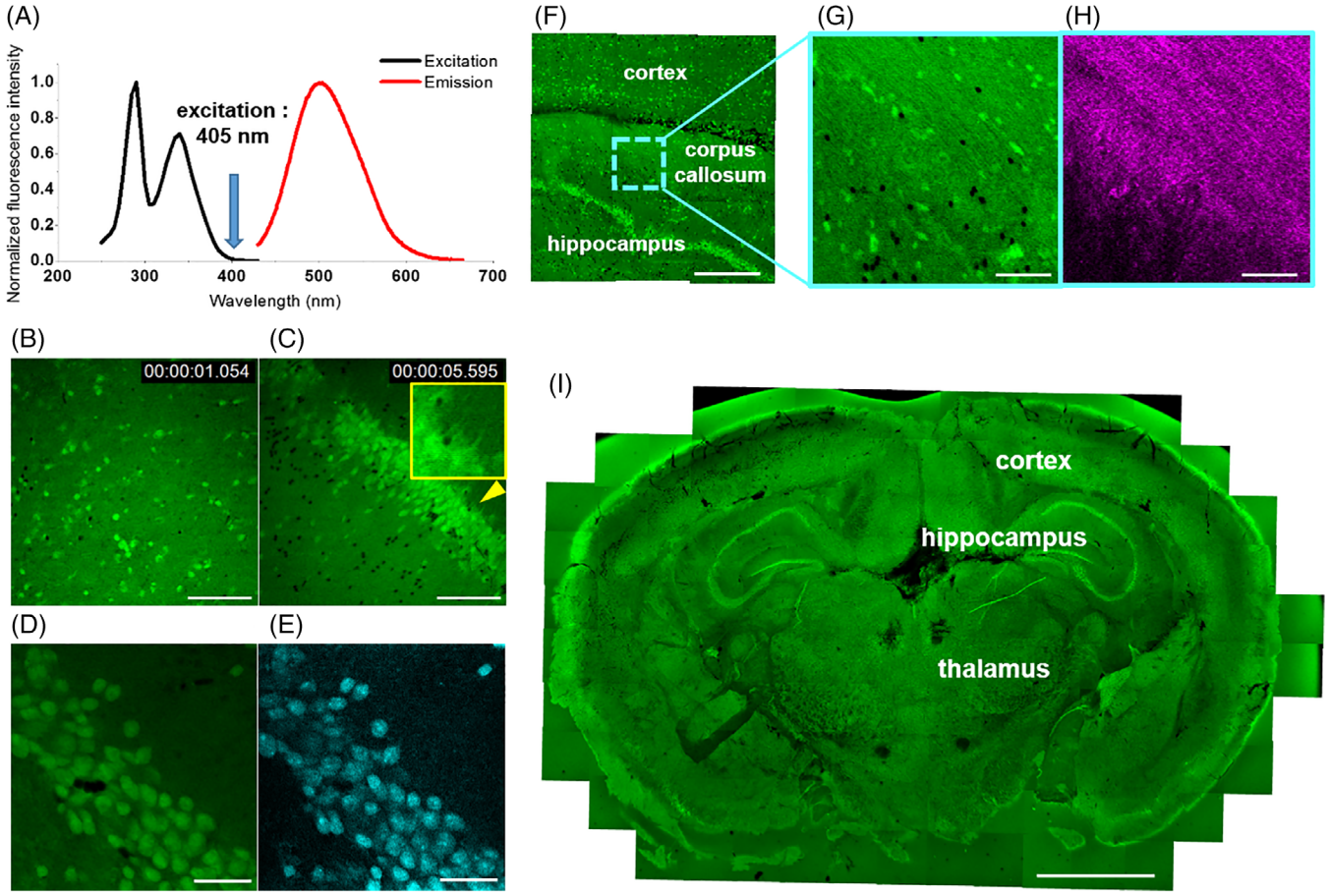

FIGURE 1 Single-photon fluorescence spectra of moxifloxacin and moxifloxacin-based confocal images of normal mouse brains. A, Single–photon fluorescence excitation and emission spectrum of moxifloxacin ophthalmic solution. n = 5. B, C, Video-rate moxifloxacin-based confocal images of the cerebral cortex and hippocampus just below the surface, showing some cells with branches (yellow arrowhead and inset). Scale bar indicates 100 μm. D, E, Moxifloxacin and acridine orange based confocal images of the hippocampus on the surface. Scale bar indicates 30 μm. F, A moxifloxacin-based confocal image of a large region covering the cerebral cortex, corpus callosum and hippocampus just below the surface. Scale bar indicates 300 μm. G, H, Magnified moxifloxacin-based confocal and confocal reflectance images of the corpus callosum just below the surface. Scale bar indicates 50 μm. I, A moxifloxacin-based confocal image of whole mouse brain section at 15 μm deep from the surface. Scale bar indicates 2 mm

sections, ex-vivo (Figure 1B-I). Fresh mouse brain slices in the coronal plane were prepared, and confocal microscopy was conducted after the topical administration of moxifloxacin ophthalmic solution and incubation for 5 minutes. High-speed imaging was tested by increasing the excitation power with the imaging speed increase to maintain the image contrast. Video-rate (29.4 frames/second) imaging speed was achieved at an excitation power of 2.3 mW, and representative video-rate images in the cortex and hippocampus of the mouse brain are shown in Figure 1B-C (Video S1 and S2). The confocal images visualized the three-dimensional (3D) cell structure in the brain through moxifloxacin labeling. The confocal images exhibited a relatively sparse cell distribution in the cortex, and a dense and band-like cell distribution in the hippocampus. Individual cells appeared with round shapes, and some cells had thin branches (arrowhead and inset in Figure 1C). The round shapes could correspond to either cell nuclei or cell bodies. The images exhibited a level of background intensity when compared to non-cellular parts of the brain, and the background was owing to intercellularly distributed moxifloxacin. Additional black round structures were observed in the moxifloxacin-based brain images, and they corresponded to RBCs not labeled by moxifloxacin. The imaging speed could not exceed the video-rate owing to limitation of the commercial confocal imaging system. Moxifloxacin labeling of cells in the normal brain was analyzed and compared with that of a cell nucleus labeling dye, acridine orange. Having a relatively long emission wavelength, the emission of acridine orange was easily separated from that of moxifloxacin. A brain slice was labeled with both moxifloxacin and acridine orange, and imaged through confocal microscopy (Figure 1D-E). The moxifloxacin-based confocal image of the brain cells matched well with the acridine orange-based confocal image, thereby indicating that MBCM mainly visualized the cell nucleus of brain cells.

Video-rate MBCM of the corpus callosum in the mouse brain exhibited fibrous structures aligned in a direction, and the fibrous structures could correspond to myelinated axons (Figure 1F-G). Confocal reflectance microscopy was conducted in the same sample for verification purposes because it adequately visualized myelinated axons owing to lipid composition and strong light reflection [21]. A confocal reflection image (Figure 1H) was well matched with the MBCM image. Therefore, it was concluded that MBCM also visualized myelinated axons in the normal brain.

High imaging speed through moxifloxacin labeling allowed the imaging of large areas of the brain, and the capability of MBCM was demonstrated through imaging the whole-brain section (Figure 1I). A mouse brain slice in the coronal section was imaged in a raster fashion by using a motorized sample stage. The whole-brain section (wherein the size was 13.3 × 8.4 mm^2 approximately) was captured in a mosaic image consisting of 144 sections (approximately 14 × 10). Individual sections were imaged in 3D from the surface to a depth of 50 μm with a step size of 1 μm. The total imaging time corresponded to 13 minutes. A whole-brain section image, which was in a single superficial plane, exhibited gross cellular structure. Various brain compartments, such as the cortex and hippocampus, were easily identified solely based on moxifloxacin fluorescence intensity. The hippocampus appeared bright owing to a dense cell arrangement. Other parts of the brain including the cortex exhibited less moxifloxacin fluorescence than the hippocampus owing to relatively low cell densities. MBCM visualized the cellular structure of the whole mouse brain slice owing to enhanced fluorescence and imaging speed.

3.3 | MBCM of brain tumor mouse models

Following the demonstration of high-speed imaging and the characterization of moxifloxacin labeling in the normal brain, MBCM was applied to brain tumor mouse models to test the feasibility of brain tumor delineation. Preparation and imaging protocols were explained in the method section. In brief, cancer cells expressing DsRed protein were implanted in the mouse brain such that the location and distribution of cancer cells were easily traced through DsRed fluorescence imaging. MBCM was conducted on fresh brain slices of the brain tumor mouse models, and results are shown in Figure 2. A bright-field image of a brain slice from the brain tumor mouse model exhibited a dark region on the left side (Figure 2A). A corresponding wide-field DsRed fluorescence image confirmed the dark region as a tumor (Figure 2B). The tumor appeared dark in the bright-field image, and this is partly owing to the occupation of transparent cancer cells and disruption of highly scattering myelinated neuronal axons. MBCM was conducted on a region covering the tumor and tumor-neighboring area in the brain slice as denoted by a green box in Figure 2A,B. Moxifloxacin and DsRed fluorescence were simultaneously imaged on two detection channels. Large-sectional mosaic confocal images in the moxifloxacin and DsRed channels are shown in Figure 2C-D, respectively. The large-sectional images exhibited the distribution of an implanted tumor in both channels. The large-sectional image in the moxifloxacin channel exhibited a high-intensity structure on the left side (Figure 2C). The structure was assumed as a tumor owing to high moxifloxacin fluorescence associated with high-density moxifloxacin labeled cells. The corresponding DsRed channel image also indicated that the fluorescent structure in the moxifloxacin channel expressed strong DsRed fluorescence, thereby confirming that it corresponded to a tumor (Figure 2D). Magnified confocal images at several regions of interest (ROIs) exhibited detail cellular structures. Magnified images at ROI-1 (which was inside the high-intensity structure) exhibited densely distributed and elongated cells in the moxifloxacin channel (Figure 2E). Significant moxifloxacin fluorescence at ROI-1 was owing to the dense cell distribution. The corresponding image in the DsRed channel exhibited high-density elongated cancer cells, thereby confirming that ROI-1 was located inside the tumor (Figure 2H). The density of cancer cells in the DsRed channel image was lower than that in the moxifloxacin channel image, and this was partly because the DsRed expression levels of cancer cells were not uniform, and additional cells including inflammatory cells beside cancer cells could be present. Magnified images at ROI-2 (which was on the right side of the large-sectional image with low moxifloxacin fluorescence) exhibited sparsely distributed cells in the moxifloxacin channel (Figure 2F) and the absence of a signal in the DsRed channel (Figure 2I). Therefore, ROI-2 corresponded to the normal region. Furthermore, ROI-3 was located on the tumor boundary, and the moxifloxacin channel image exhibited two distinctive regions of high fluorescence intensity and dense cells on the upper left side, and relatively low fluorescence intensity and less dense cell distribution on the lower right side (Figure 2G). The two regions with different cell densities and fluorescence intensities in the moxifloxacin channel image were confirmed as tumor and normal regions by the corresponding DsRed channel image (Figure 2J). In the mouse model, MBCM easily detected the implanted tumor and its boundary based on moxifloxacin fluorescence intensity and cellular structure.

3.4 | MBCM of malignant human brain tumor specimens

After the testing of tumor delineation in the brain tumor mouse model, MBCM was applied to human brain tumor specimens, ex-vivo. Two different types of malignant human

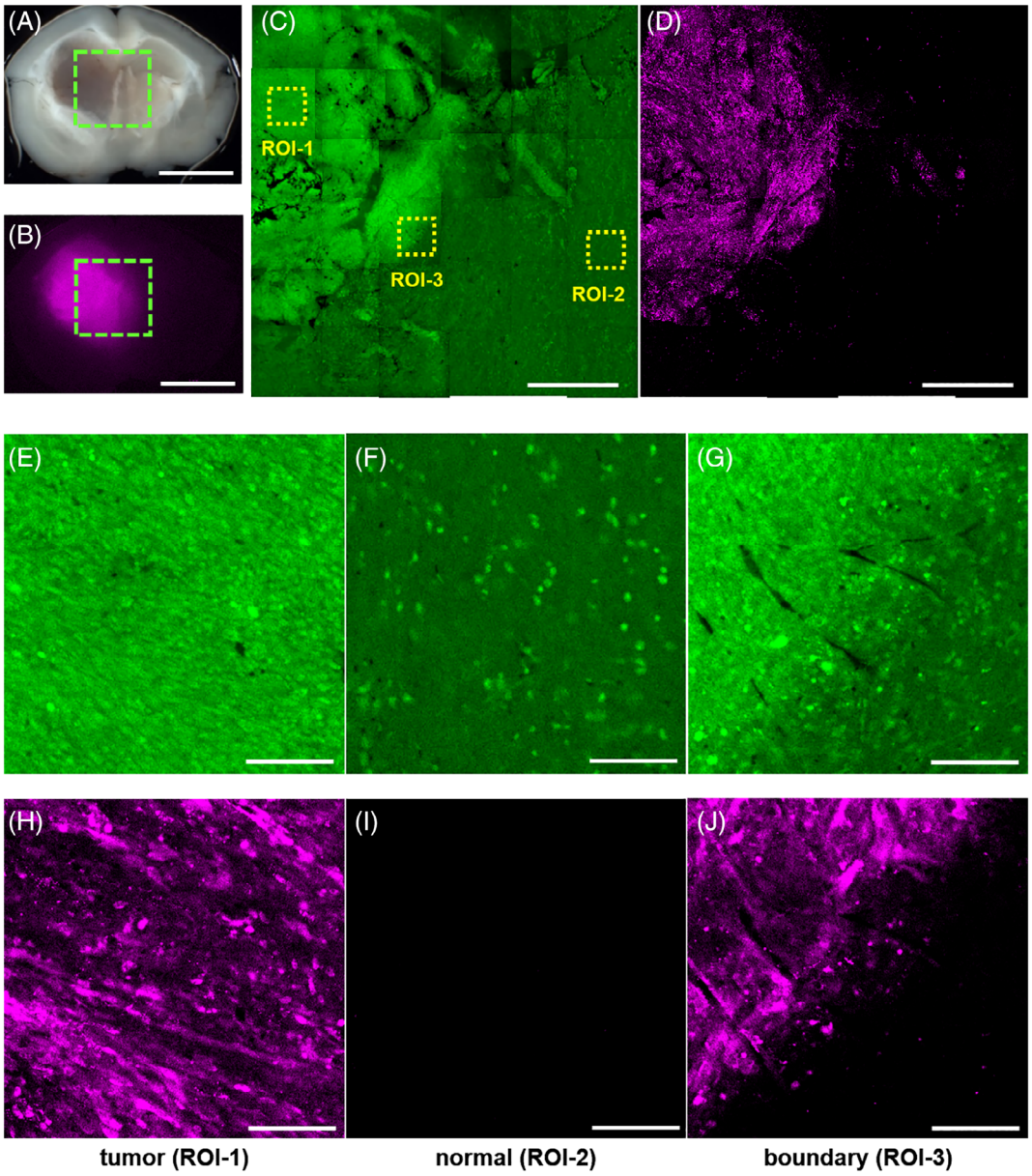

FIGURE 2 Bright-field, wide-field fluorescence, and moxifloxacin/DsRed based confocal images of a brain tumor mouse model, ex-vivo. A, B, A bright-field image of a mouse brain slice containing DsRed protein-expressing cancer cells and a corresponding wide-field DsRed fluorescence image of the mouse brain slice. Scale bar indicates 3 mm. C,D, Large-sectional mosaic moxifloxacin-based and DsRed-based confocal images just below the surface. Scale bar indicates 1 mm. E-G And H-J, Magnified moxifloxacin-based and DsRed-based confocal images in the tumor, normal, and tumor-boundary region, respectively. Scale bar indicates 100 μm

brain tumors were examined, glioblastoma and metastatic cancer. MBCM was conducted on the human brain tumor specimens in a manner similar to the mouse model case. The first human case was glioblastoma, and the study results including MBCM images are shown in Figure 3. A bright-field microscopy image that was acquired before MBCM imaging exhibited two distinctive regions (Figure 3A). There were a translucent and red-colored region, and a white-colored region. MBCM was conducted in a green boxed area of the specimen in the bright-field image to capture both the translucent and whitish regions. The MBCM image exhibited two regions expressing different fluorescence intensities (Figure 3B). The high- and low-intensity regions were confirmed as the tumor and tumor-neighboring regions, respectively, through a corresponding histological image (Figure 3C). Magnified images at several ROIs exhibited cellular information. Three ROIs including an ROI inside the high fluorescence intensity tumor (ROI-1), an ROI outside the tumor (ROI-2), and an ROI on the tumor-boundary (ROI-3) were selected, and the magnified images were presented. The magnified MBCM image at ROI-1 exhibited high-density cells labeled with moxifloxacin (Figure 3D). A

corresponding histological image exhibited dense cancer cells similar to the MBCM image (Figure 3G). At the neighboring region of the tumor (ROI-2), an MBCM image exhibited sparsely distributed cells (Figure 3E) as shown by a corresponding histological image (Figure 3H). However, the histological image at ROI-2 detected normal cells and a multinucleated cancer cell as denoted by a yellow arrowhead. Detection of the cancer cell at ROI-2 indicated infiltration of glioblastoma cancer cells into the tumor-neighboring region, and this implies that ROI-2 corresponded to a tumor-infiltrating neighboring region and not a normal region. Close examination of the MBCM image also indicated a multinucleated cell, denoted by a yellow arrow head. Further analysis would be needed to verify whether the cell was a cancer cell. On the boundary of the tumor (ROI-3), an MBCM image exhibited two regions

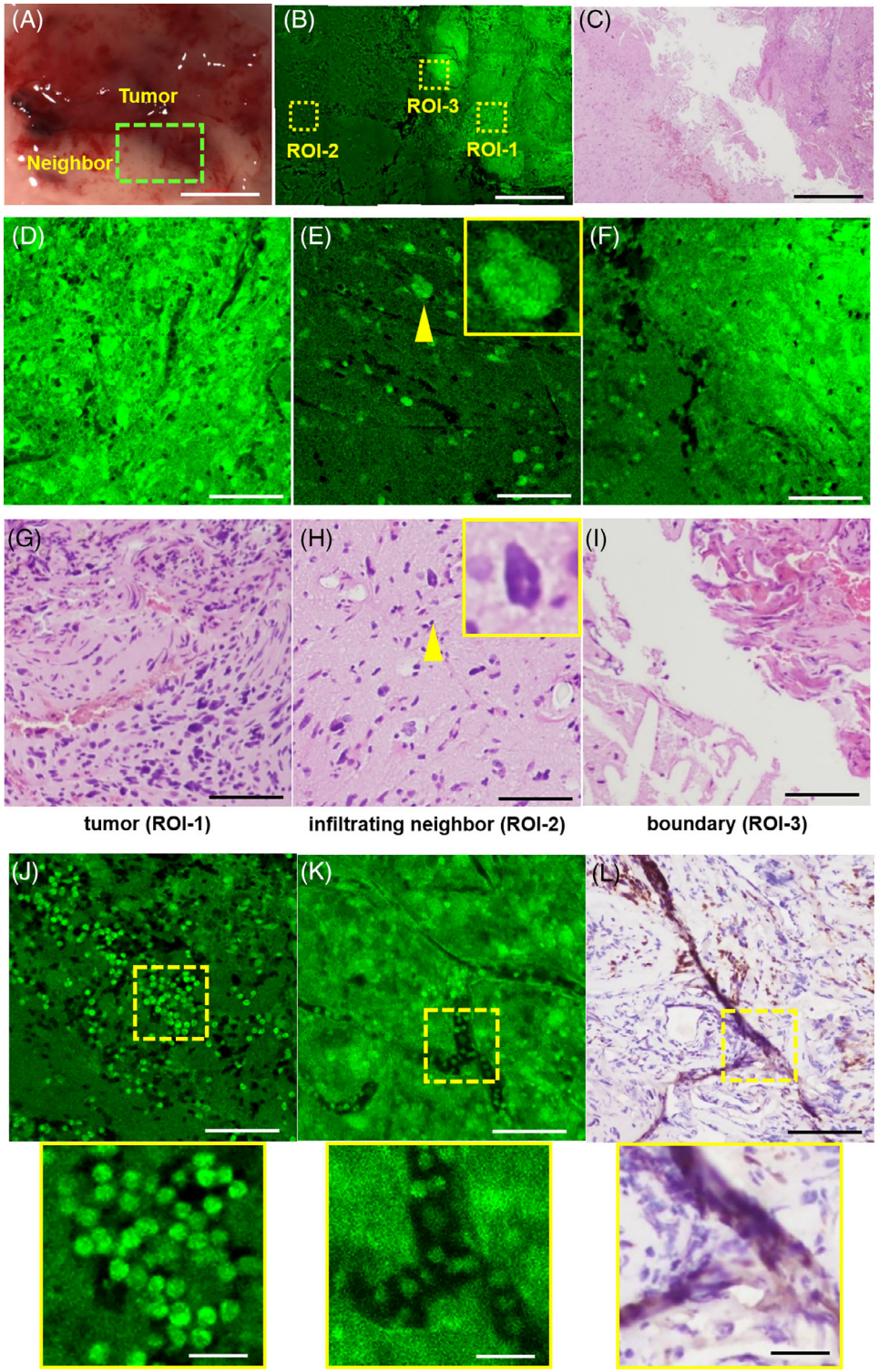

FIGURE 3 Bright-field, moxifloxacin-based confocal, and histological images of a human glioblastoma specimen. A, A bright-field image of a human glioblastoma specimen. Scale bar indicates 4 mm. B,C, A large-sectional mosaic moxifloxacin-based confocal image on the surface and a corresponding low-magnification hematoxylin and eosin-stained histological image. Scale bar indicates 1 mm. D-F and G-I, Magnified moxifloxacin-based confocal images and corresponding high-magnification hematoxylin and eosin-stained histological images in the tumor, tumor-infiltrating neighbor and tumor-boundary region, respectively, including multinucleated cancer cells (yellow arrowheads). Scale bar indicates 100 μm. (J, K) Magnified moxifloxacin-based confocal images in a tumor-neighboring region and in the tumor region, respectively. Scale bar indicates 100 μm. Imaging depths for (J, K) are 0 and 8 μm deep from the surface, respectively. Round shape cells in yellow dashed boxes were zoomed as shown in below figures. Scale bars indicate 50 μm. L, High-magnification hematoxylin, eosin and CD3 (brown color) stained histological image in the tumor region. Scale bar indicates 100 μm. CD3 stained T-cells were zoomed as shown in a below figure. Scale bars indicate 50 μm

with different fluorescence intensities and cell densities (Figure. 3F). A corresponding histological image on the tumor boundary exhibited the two different regions although the specimen in the histological image was torn apart as an artifact of histology processing (Figure 3I). Additionally, MBCM exhibited round-shaped cells with bright fluorescence near the tumor boundary (Figure 3J). Round fluorescent cells were also found inside blood vessels in the tumor region (Figure 3K) and extracted peripheral blood (Figure S2). Based on the shape and location, the round cells were considered as WBCs, such as T-cells, recruited as an immune response to tumor. A histological image of the tumor region using CD3 antibody for T-cell staining (brown color) exhibited the presence of several T-cells inside blood vessels (Figure 3L). A further examination would be required for the identification of the round cells.

The second case was a human metastatic cancer specimen. MBCM was conducted in fresh condition, and the results are shown in Figure 4. A large-sectional MBCM image and a corresponding low-magnification histological image are shown in Figure 4A,B, respectively. Both the MBCM image and histological image exhibited clear distinction between tumor and tumor-neighboring regions. In the MBCM image, the tumor region exhibited significant fluorescence when compared to the neighboring region owing to high cell density. The corresponding histological image exhibited a cancer distribution similar to the MBCM image although the two images were slightly mismatched. This mismatch was owing to tissue loss and deformation during histology processing. The histological image exhibited an arrangement of cancer cells resembling the typical morphology of epithelial cells in the stomach from which the cancer cells originated. With respect to the detailed examination, three ROIs were chosen, namely the first ROI inside the tumor (ROI-1), second ROI in the tumor-neighboring region (ROI-2), and third ROI on the tumor boundary (ROI-3). At ROI-1 that was inside the tumor, an MBCM image exhibited densely distributed cells indicating cancer cells (Figure 4C), and this was confirmed by a corresponding histological image (Figure 4F). Arrangement of cancer cells in the MBCM image was similar to an MBCM image at a stomach (Figure S3), which implied this cancer came from stomach. At ROI-2 that corresponded to the tumor-neighboring region, an MBCM image exhibited sparsely distributed cells (Figure 4D), and it was consistent with a corresponding histological image (Figure 4G), thereby confirming ROI-2 as a normal region. At ROI-3 that was on the tumor-boundary, high-density cells were observed on the upper side of the MBCM image (Figure 4E), and this was consistent with corresponding histological image (Figure 4H). Cancer cells were individually resolved, and their arrangement was recognized. A group of clustered cells in the tumor-neighboring region as denoted by a yellow arrowhead and magnified in an inset in Figure 4A exhibited a cell arrangement similar to those on the tumor boundary in ROI-3. The histological image confirmed that the group of clustered cells corresponded to infiltrating cancer cells as denoted by a yellow arrowhead in Figure 4B.

3.5 | Image analysis of MBCM images of tumor specimens

With respect to the automated detection of tumors from MBCM images, an image analysis method was developed (Figure 5 and Figure S4). Tumor regions exhibited high moxifloxacin fluorescence intensities when compared to normal brain regions or tumor-infiltrating neighbor regions owing to high cell density. Thus, an intensity-based image analysis method was devised. Large-sectional MBCM images were divided into small image windows consisting of 128 × 128 pixels with a size of 96.9 x 96.9 μm^2, and the image windows were analyzed in intensity histograms. Representative image windows of the tumor region and neighboring normal brain region, their intensity histograms, and a two-dimensional (2D) scattering plot obtained through image analysis are shown in Figure 5A and Figure S4. Histograms of the tumor and normal brain image windows exhibited different intensity distributions. The histogram of the normal brain image window exhibited a relatively low and narrow intensity distribution when compared to that of the tumor image window. Specifically, the histogram of normal brain window exhibited the maximum frequency at the intensities of background image pixels associated with a sparse cell distribution in the normal brain image window. It also exhibited a relatively narrow intensity distribution owing to uniform intensities of background image pixels. Conversely, the histogram of tumor image window exhibited the maximum frequency at the intensities of cell image pixels owing to high cell density, and the intensities were higher than the background intensities. Additionally, the intensities of cell image pixels exhibited a broader distribution when compared to that of background pixel intensities owing to the higher intensity variation. The histogram of a tumor boundary image window was a combination of the two histograms of the neighboring normal and tumor image windows. From the intensity histogram analysis, two parameters were formed to separate the tumor and normal brain image windows (Figure S4,B). The first parameter corresponded to the intensity at the maximum frequency of the histogram, and the second parameter corresponded to the weighted sum of high-intensity pixels. The intensity at the maximum frequency of the histogram was straightforward because tumor image windows typically exhibit higher intensities than normal brain image windows. However, the

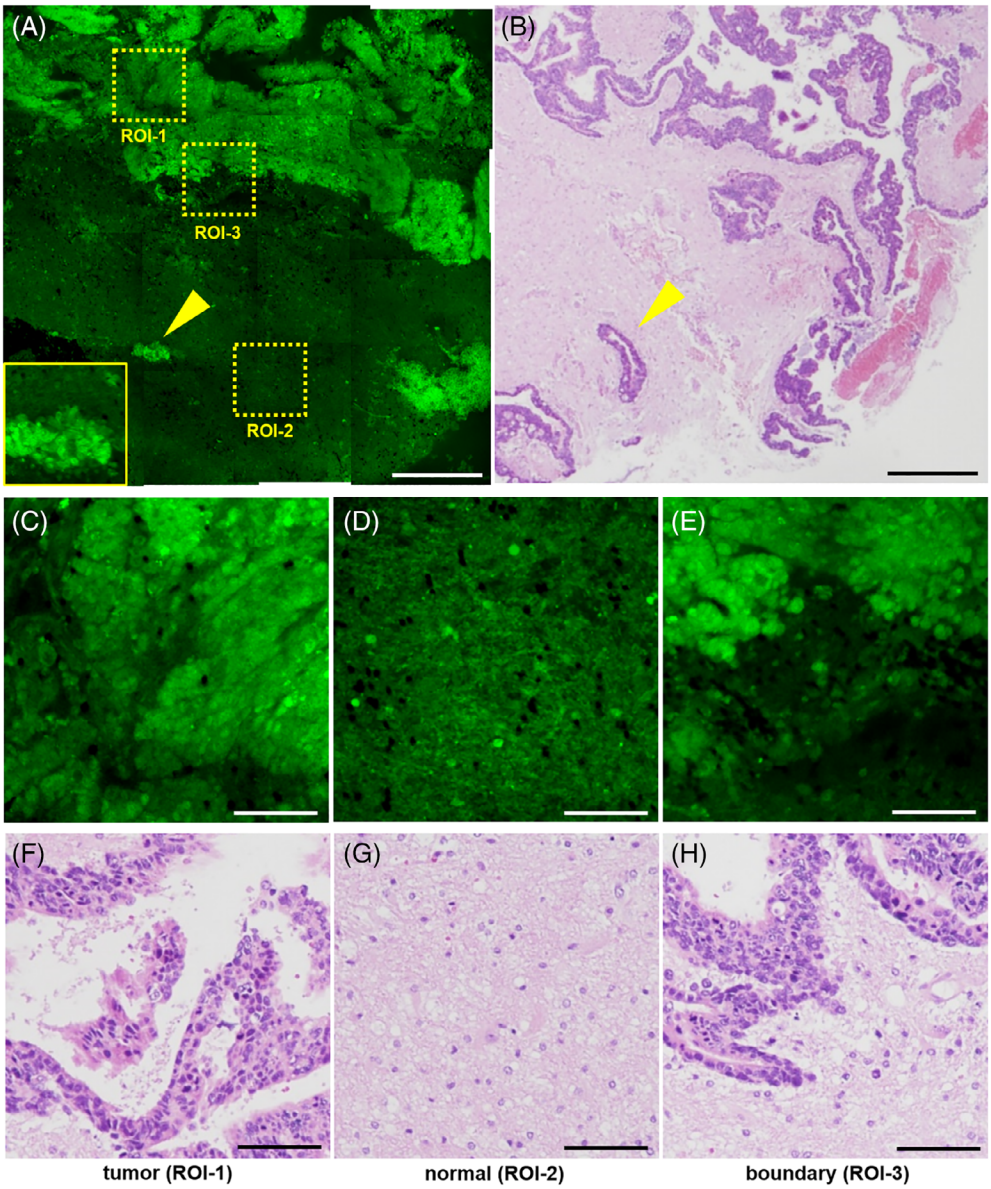

FIGURE 4 Moxifloxacin-based confocal and histological images of a human metastatic cancer specimen. A, B, A large-sectional mosaic moxifloxacin-based confocal image at 9 μm deep from the surface and a corresponding low-magnification hematoxylin and eosin-stained histological image. Infiltrating cancer cell clusters (yellow arrowheads) are shown. Scale bar indicates 500 μm. C-E and F-H, Magnified moxifloxacin-based confocal images and corresponding high-magnification hematoxylin and eosin-stained histological images in the tumor, normal, and tumor-boundary regions respectively. Scale bar indicates 100 μm

intensity at the frequency peak did not result in significant separation. Hence, the second parameter (P) was formed based on the width of intensity distribution. The weighted sum of high-intensity pixels (P) was obtained via integrating the frequency of high-intensity pixels (P_I) with a weighting factor (W_I) as shown in Eq. (1). High-intensity pixels were selected as pixels wherein intensities exceeded a threshold intensity (I_{th}), which was calculated as sum of the average intensity (m) and twice the standard deviation (σ) in a normal brain region of the MBCM image as shown in Eq. (2). The threshold was to separate high-intensity image pixels of cells from low-intensity background image pixels in the image. The weighting factor corresponded to a square of the ratio of the pixel intensity to the threshold intensity as shown in Eq. (3). The weighting factor provided more weights to the image pixels with higher intensity ratios. The analysis results of the representative tumor and neighboring normal image windows were plotted in a 2D scattering plot and shown in Figure 5A and Figure S3C. The intensity at the maximum frequency of the intensity histogram and the weighted sum of high-intensity pixels are plotted in the x and y axes, respectively. The expressions are as follows:

$$P = \int_{I_{th}}^{\infty} \left(\frac{I}{I_{th}}\right)^2 P_I dI = \int_{I_{th}}^{\infty} W_I P_I dI, \quad I \geq I_{th} \tag{1}$$

$$I_{th} = m + 2\sigma \tag{2}$$

$$W_I = \left(\frac{I}{I_{th}}\right)^2, \quad I \geq I_{th} \tag{3}$$

Small image windows (n = 64) of MBCM images in all the brain tumor specimens were analyzed, and their results

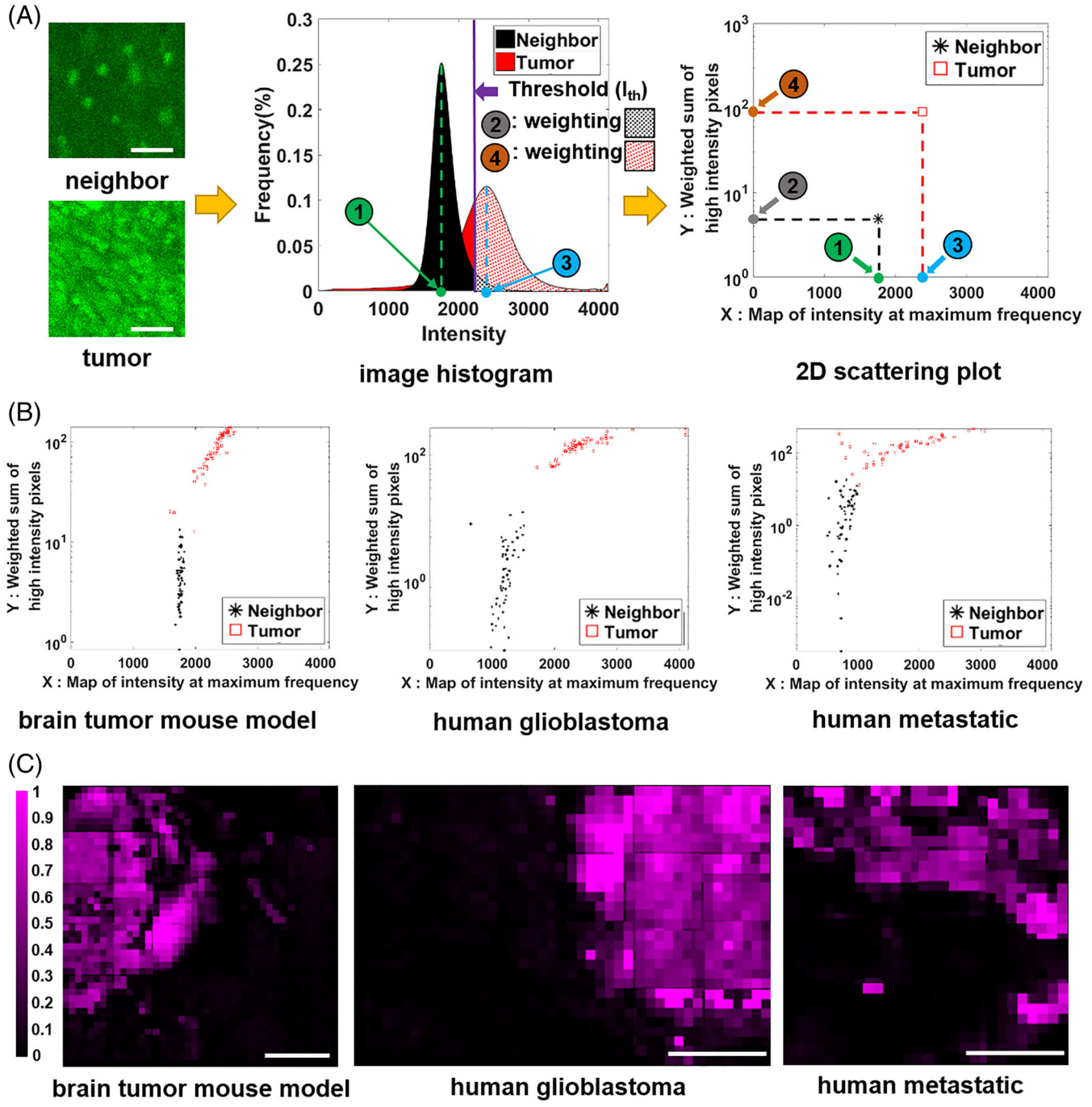

FIGURE 5 Quantitative analysis of moxifloxacin-based confocal images of brain tumor specimens. A, An image histogram and a 2D scattering plot of a representative image window (96.9 × 96.9 μm^2) in the tumor-neighboring region and tumor region, respectively. Scale bar indicates 30 μm. Detailed image analysis procedure with the image histogram and two-dimensional (2D) scattering plot was shown in Figure S4. (B) 2D scattering plots of moxifloxacin-based confocal image windows in the brain tumor specimens. n = 64. (C) Maps of the image analysis of the brain tumor mouse model, human glioblastoma, and human metastatic tumor specimens

were plotted based on the two parameters (Figure 5B). In the brain mouse tumor model, the analysis results of tumor and neighboring normal brain image windows as confirmed by the DsRed channel images were plotted. Tumor image windows appeared higher in both the *x*- and *y*-axes when compared to those in normal image windows, and their separation was more significant in the *y*-axis of the weighted sum of high-intensity pixels. In the analysis of human brain tumor specimens, image windows of the tumor and tumor-neighboring regions with tumor-infiltrating neighboring regions and normal neighboring regions in glioblastoma and metastatic specimens, respectively, were classified based on the corresponding histological image and the analysis results were shown in Figure 5B. The tumor image windows of

human brain specimens were adequately separated from the neighboring image windows. However, the analysis results were not objective. Therefore, the image analysis results were mapped on the original MBCM images as shown in Figure 5C. The image maps generated from the analysis algorithm overlapped with the original images (Figure S5), thereby indicating that the image analysis algorithm worked well.

4 | DISCUSSIONS

A high-speed high-contrast cellular imaging method for brain tumor detection and delineation was developed by using moxifloxacin and confocal microscopy. Moxifloxacin was used as a cell labeling agent for high-speed cellular imaging and examination. Although moxifloxacin had single-photon excitation peaks at UV, the excitation at the short visible wavelength of 405 nm was sufficiently strong for video-rate high-contrast confocal imaging. A small excitation power of 2.3 mW was used in the video-rate confocal imaging, and the power was approximately 100 times less than that of damage threshold [22]. MBCM of the normal brain tissue visualized individual cells and especially either the cell nuclei or cell bodies of brain cells through strong moxifloxacin labeling. In the normal brain tissue, MBCM exhibited a map of regular cell distribution with varying cell densities throughout the brain slice. Cells were distributed sparsely in most of the brain compartments with the exception of the hippocampus. However, the cell distribution was significantly regular in the normal brain. After the characterization in the normal mouse brain, MBCM was applied to brain tumor specimens of the mouse model and human patients. The brain tumor mouse model was generated through implanting DsRed protein-expressing cancer cells in the brain such that the results of MBCM were confirmed by DsRed fluorescence images of cancer cells. Two types of malignant human brain tumor specimens, glioblastoma and metastatic cancer, were imaged in large sections to capture their boundaries, and the results were compared with histology. MBCM detected tumors by visualizing cellular structures different from those of the normal brain. Tumors exhibited dense and irregular cell distributions in all the cases. Given high cell densities, tumor regions exhibited higher intensities of moxifloxacin fluorescence when compared to normal or tumor-infiltrating neighboring regions in low-magnification moxifloxacin-based images. Cellular information, such as cell orientation and distribution, was obtained by 3D confocal imaging.

Although MBCM easily detected tumor regions based on high moxifloxacin fluorescence and irregular dense cell distribution, the results of human brain tumor study also involved a few challenges in the detection of infiltrating cancer cells. In the case of human glioblastoma, MBCM did not easily detect infiltrating cancer cells that were observed as either alone or grouped as a few in the region of sparsely distributed normal cells. Although MBCM captured the multinucleated cancer cells, the image did not exhibit sufficient contrast to discern multinucleated cancer cells from the clusters of a few normal cells in contrast to hematoxylin and eosin histology. However, this limitation is common to all other microscopy techniques. Although MBCM could not detect isolated multinucleated glioblastoma cancer cells, it easily detected the group of infiltrating cancer cells in the case of metastatic cancer. This was simply because the cancer cells infiltrated as a large group. Therefore, the sensitivity limitation of MBCM could be set by either the area or number of grouped cancer cells. Further studies including more sample imaging and the development of image analysis are required for verification and confirmation.

In MBCM, additional cellular features were observed in the two human brain tumor cases. In the human glioblastoma case, MBCM results indicated a different type of cells that were scattered near the tumor boundary. The cells were round in shape and exhibited significant moxifloxacin fluorescence. Similar cells were found inside the blood vessel of the brain tumor (Figure 3K) and extracted peripheral blood (Figure S2). The cells were considered as leukocytes (for eg, T-cells) that result from the immune response to tumor. In the case of human metastatic cancer specimen, MBCM visualized cancer cells that were arranged in a specific way on the tumor boundary. The arrangement of cancer cells corresponded to villus structures resembling their origin, namely the stomach epithelium. Similar cellular structures were imaged in the freshly excised mouse stomach specimen via MBCM (Figure S3). Infiltrating cancer cells were detected considerably easily in the metastatic cancer case because the cancer cells formed a relatively large group and a distinctive cell arrangement potentially owing to their origin. The findings should also be further examined with more samples and image processing for confirmation.

Detection of tumors through MBCM was considerably straightforward because tumors exhibited significant moxifloxacin fluorescence and irregular and dense cell distribution. An automated detection algorithm of tumors was developed based on an intensity histogram of the image. The intensity histogram of tumor regions exhibited high and broad intensity distribution owing to the abundance of moxifloxacin labeled cells while that of tumor-neighboring regions exhibited relatively low and narrow intensity distribution owing to a sparse cell distribution and abundance of background. The differences in the intensity histogram were processed as a 2D scatter plot, and all the MBCM images of brain tumor tissues exhibited distinctive separation of tumors and tumor-neighboring tissues. The intensity-based image

analysis method worked well in detecting tumor regions although there is room for improvement in the future via utilizing cell morphology information.

The intensity-based image analysis showed that fluorescence intensity alone could detect tumors. Although confocal microscopy was used in this study, wide-field fluorescence imaging techniques without 3D resolution might be able to detect tumors in principle based on fluorescence intensity difference. However, we still prefer high-resolution 3D fluorescence microscopy like confocal microscopy over wide-field fluorescence microscopy for sensitive and accurate detection of brain tumors. MBCM could visualize irregular and dense cellular structures in tumors and distinguished tumors from normal brain tissues based on cellular structure. In the case of the normal brain, MBCM visualized sparse cell distributions in most of brain regions, and dense and regular cell distributions in specific regions such as the hippocampus. Fluorescence intensity alone might not be able to distinguish tumors from the normal regions with dense and regular cell distribution. MBCM requires topical moxifloxacin administration prior the imaging, and wide-field fluorescence imaging techniques could be sensitive to artifacts of the moxifloxacin labeling. In the current labeling procedure, brain tissue specimens were not washed after topical administration and there was residual moxifloxacin on the tissue surface. Residual moxifloxacin on the surface was not a serious problem for confocal microscopy owing to its 3D sectioning capability, but it could be for wide-field fluorescence imaging. The washing step could be difficult in real in-vivo applications. There could be additional variations in the labeling as well. Confocal microscopy examination would not be sensitive such artifacts and might be able to detect brain tumors robustly.

Different imaging parameters were used in MBCM imaging of the normal brain and brain tumor specimens. The brain tumor specimens were imaged at the relatively low imaging speed of 0.27 frames/second with the large FOV and high pixel number ($775 \times 775\ \mu m^2$ and 1024×1024 pixels), while the normal brain specimens were imaged at 29.4 frames/second with the relatively small FOV and small pixel number ($387.5 \times 387.5\ \mu m^2$, 512×512 pixels). Because MBCM generated enough fluorescence signal for video-rate imaging, the brain tumor specimens could be imaged at the same high speed as well. But we initially focused to obtain high quality and large FOV images of brain tumors rather than to image the specimens fast. Later, we imaged brain tumor specimens at the high speed without much contrast degradation. Therefore, high-speed MBCM imaging could be applied to any brain tissue specimens.

In the current study, 405 nm wavelength was used for moxifloxacin excitation and MBCM imaging. Although the excitation efficiency of moxifloxacin at 405 nm was only approximately 0.5% compared to the one at the peak excitation wavelength, MBCM could image brain tissues at 29.4 frames/second, which was much faster than the typical imaging speed of TPM. Two-photon excitation is usually many orders of magnitude lower than single-photon excitation, and femtosecond pulse lasers are used to increase fluorescence signal to reasonable levels for imaging. Fluorescence intensities in the two different excitation conditions were compared. A femtosecond Ti-Sapphire laser (Chameleon Vision, Coherent) was used for two-photon excitation. 405 and 700 nm were used as single-photon and two-photon excitation wavelengths, respectively. At the same excitation power of 1 mW, fluorescence intensity with single-photon excitation at 405 nm was approximately 690 times higher than the intensity with two-photon excitation at 700 nm. Even if the power for two-photon excitation was increased to 5 mW, which is typical power level for in-vivo TPM imaging in the skin, single-photon excitation at 405 nm was still stronger than two-photon excitation by approximately 28 times. Therefore, confocal microscopy with 405 nm excitation wavelength provided much higher fluorescence signal than TPM in the moxifloxacin labeled specimens. Further fluorescence signal enhancement could be achieved simply by using the second peak single-photon excitation wavelength of 340 nm in the custom confocal microscopy system.

MBCM provided cellular information of the normal brain and brain tumor with high correlation with histology. However, MBCM provides mainly morphological information on cells and does not provide specific information like other techniques, such as histology or molecular imaging. However, the main advantage of the method is its potential for direct application on human tissue in the surgical field without excision by using clinically compatible moxifloxacin as the labeling agent. With respect to improvements in the sensitivity, additional labeling agents could be used in conjunction with moxifloxacin, and imaging would be possible only in excised tissues. In the study, all the MBCM tests were conducted in ex-vivo fresh brain tissues. However, its application to human patients and exposed brain tissue in surgical field during surgery would be fundamentally possible by using clinically compatible moxifloxacin. A portable confocal imaging device is required with respect to the direct imaging of the exposed brain tissue in the surgical field. This can be solved by using commercially available CLE. Moxifloxacin ophthalmic solution was topically administered on the specimens, and the incubation time was less than 5 minutes owing to the high tissue penetration of moxifloxacin. The method is simple and effective, and there are no significant technical barriers in proceeding to a clinical study. The next step involves either pre-clinical or clinical studies by adapting the existing CLE.

5 | CONCLUSIONS

A high-speed high-contrast cellular imaging method was developed based on clinically compatible moxifloxacin as a cell labeling agent and confocal microscopy for sensitive brain tumor detection and delineation. The novel usage of moxifloxacin allowed high-speed cellular imaging and rapid examination of cellular structure in tissues. The application of MBCM to brain tumor specimens including malignant human brain tumors indicated a clear distinction of brain tumors from the tumor-surrounding brain region, and the study revealed the potential of MBCM application to brain tumor delineation in a clinical setting.

ACKNOWLEDGMENTS

The study was supported in part by the Industrial Technology Innovation Program (No.10048358) funded by the Ministry of Trade, Industry & Energy of the Korean Government; the Brain Research Program (NRF-2017M3C7A 1044964) funded by the Ministry of Science & ICT & Future Planning of the Korean Government through the National Research Foundation (NRF) of Korea; the Korea–Sweden Research Cooperation Program (2017R1A2A1A18070960) and the research grant (NRF-2016R1A2B4015381) of the NRF funded by the Korean Government.

ORCID

Ki Hean Kim https://orcid.org/0000-0003-3410-7706

REFERENCES

[1] M. Lacroix, D. Abi-Said, D. R. Fourney, Z. L. Gokaslan, W. Shi, F. DeMonte, F. F. Lang, I. E. McCutcheon, S. J. Hassenbusch, E. Holland, K. Hess, C. Michael, D. Miller, R. Sawaya, *J. Neurosurg.* **2001**, *95*, 190.

[2] M. J. McGirt, D. Mukherjee, K. L. Chaichana, K. D. Than, J. D. Weingart, A. Quinones-Hinojosa, *Neurosurgery* **2009**, *65*, 463.

[3] D. J. Engle, L. D. Lunsford, *J. Neurooncol* **1987**, *4*, 361.

[4] D. Liang, M. Schulder, *Surg. Neurol. Int.* **2012**, *3*, S320.

[5] R. Sastry, W. L. Bi, S. Pieper, S. Frisken, T. Kapur, W. Wells III., A. J. Golby, *J. Neuroimaging* **2017**, *27*, 5.

[6] M. M. Haglund, M. S. Berger, D. W. Hochman, *Neurosurgery* **1996**, *38*, 308.

[7] W. Stummer, U. Pichlmeier, T. Meinel, O. D. Wiestler, F. Zanella, H.-J. Reulen, A.-G. S. Group, *Lancet Oncol.* **2006**, *7*, 392.

[8] A. H. Zehri, J. F. G. Wyatt Ramey, M. A. Mooney, N. L. Martirosyan, M. C. Preul, P. Nakaji, *Surg. Neurol. Int.* **2014**, *5*, 60.

[9] D. Milej, A. Abdalmalak, L. Desjardins, H. Ahmed, T.-Y. Lee, M. Diop, K. S. J. S. R. Lawrence, *Sci. Rep.* **2017**, *7*, 1702.

[10] P. A. Valdés, Z. B. Moses, A. Kim, C. J. Belden, B. C. Wilson, K. D. Paulsen, D. W. Roberts, B. T. Harris, *J. Neuropathol. Exp. Neurol.* **2012**, *71*, 806.

[11] C. Kut, K. L. Chaichana, J. Xi, S. M. Raza, X. Ye, E. R. McVeigh, F. J. Rodriguez, A. Quiñones-Hinojosa, X. Li, *Sci. Transl. Med.* **2015**, *7*, 292ra100.

[12] M. Ji, D. A. Orringer, C. W. Freudiger, S. Ramkissoon, X. Liu, D. Lau, A. J. Golby, I. Norton, M. Hayashi, N. Y. Agar, G. S. Young, C. Spino, S. Santagata, S. Camelo-Piragua, K. L. Ligon, O. Sagher, X. S. Xie, *Sci. Transl. Med.* **2013**, *5*, 201ra119.

[13] O. Uckermann, R. Galli, S. Tamosaityte, E. Leipnitz, K. D. Geiger, G. Schackert, E. Koch, G. Steiner, M. Kirsch, *PLoS One* **2014**, *9*, e107115.

[14] V.-H. Le, S. W. Yoo, Y. Yoon, T. Wang, B. Kim, S. Lee, K.-H. Lee, K. H. Kim, E. Chung, *Biomed. Opt. Express* **2017**, *8*, 2148.

[15] R. D. Gosling, L. O. Uiso, N. E. Sam, E. Bongard, E. G. Kanduma, M. Nyindo, R. W. Morris, S. H. Gillespie, *Am. J. Respir.* **2003**, *168*, 1342.

[16] D. Miller, *Clin. Ophthalmol* **2008**, *2*, 77.

[17] J. A. Ocaña, F. J. Barragán, M. Callejón, *Analyst* **2000**, *125*, 2322.

[18] T. Wang, W. H. Jang, S. Lee, C. J. Yoon, J. H. Lee, B. Kim, S. Hwang, C.-P. Hong, Y. Yoon, G. Lee, V.-H. Le, S. Bok, G. O. Ahn, J. Lee, Y. S. Gho, E. Chung, S. Kim, M. H. Jang, S.-J. Myung, M. J. Kim, P. T. C. So, K. H. Kim, *Sci. Rep.* **2016**, *6*, 27142.

[19] S. Lee, J. H. Lee, T. Wang, W. H. Jang, Y. Yoon, B. Kim, Y. W. Jun, M. J. Kim, K. H. Kim, *Sci. Rep.* **2018**, *8*, 9415.

[20] J. Bucevičius, G. Lukinavičius, R. Gerasimaitė, *Chem* **2018**, *6*, 18.

[21] A. J. Schain, R. A. Hill, J. Grutzendler, *Nat. Med.* **2014**, *20*, 443.

[22] P. Ramakrishnan, M. Maclean, S. J. MacGregor, J. G. Anderson, M. H. Grant, *Toxicol. In Vitro* **2016**, *33*, 54.

SUPPORTING INFORMATION

Additional supporting information may be found online in the Supporting Information section at the end of this article.

How to cite this article: Lee S, Park WY, Chang H, et al. Fast and sensitive delineation of brain tumor with clinically compatible moxifloxacin labeling and confocal microscopy. *J. Biophotonics*. 2020;13: e201900197. https://doi.org/10.1002/jbio.201900197